Bioorganic Chemistry 101 (2020) 103989

Contents lists available at ScienceDirect

Bioorganic Chemistry

journal homepage: www.elsevier.com/locate/bioorg

New complex polycyclic compounds: Synthesis, antiproliferative activity and mechanism of action

Giuseppe Daidone[a,1], Antonella D'Anneo[b,1], Maria Valeria Raimondi[a,*,1], Demetrio Raffa[a], Ernest Hamel[d], Fabiana Plescia[a,*], Marianna Lauricella[c,2], Benedetta Maggio[a,2]

[a] Department of Biological, Chemical and Pharmaceutical Sciences and Technologies (STEBICEF), Medicinal Chemistry and Pharmaceutical Technologies Section – University of Palermo, Via Archirafi 32, 90123 Palermo, Italy
[b] Department of Biological, Chemical and Pharmaceutical Sciences and Technologies (STEBICEF), Laboratory of Biochemistry, University of Palermo, Via del Vespro 129, 90127 Palermo, Italy
[c] Department of Biomedicine, Neurosciences and Advanced Diagnostics (BIND), Institute of Biochemistry, University of Palermo, Via del Vespro 129, 90127 Palermo, Italy
[d] Screening Technologies Branch, Developmental Therapeutics Program, Division of Cancer Treatment and Diagnosis, Frederick National Laboratory for Cancer Research, National Cancer Institute, National Institutes of Health, Frederick, MD 21702, United States

ARTICLE INFO

Keywords:
O-glycoconjugate polycyclic compounds
Pyrazolo[3,4-*b*]pyrazolo[3′,4′:2,3]azepino[4,5-*f*]azocine
Antiproliferative activity
MDA-MB231 breast cancer cells
Autophagy
Apoptosis

ABSTRACT

Polycyclic or *O*-glycoconiugate polycyclic compounds **1a-g** were previously tested for their in vitro antiproliferative activity. In this series of compounds, activity increases as log P decreases. Specifically, compounds **1d** and **1g** showed lower log P values together with the best antiproliferative profiles. With the aim of extending our understanding of the structure–activity relationship (SAR) of this class of compounds, we prepared new polycyclic derivatives **2a-c**, which bear on each of the two phenyl rings hydrophilic substituents (OH, SO_2NH_2 or $NHCOCH_3$). These substituents are able to form hydrogen bonds and to decrease the partition coefficient value as compared with compound **1d**. Compound **2a** was slightly more active than **1d**, while **2b** and **2c** had antiproliferative activity comparable to that of **1d**. Finally, the role of the two phenyl groups of polycycle derivatives **1** was also investigated. The analog **3**, which bears two methyls instead of the two phenyls had a lower log P value (2.94 ± 1.22) than all the other compounds, but it had negligible antiproliferative activity at 10 μM. The analysis of the most active derivative **2a** revealed a significant antiproliferative activity against the triple-negative breast cancer cell line MDA-MB231. After a 24 h treatment, an autophagic process was activated, as demonstrated by an increase in monodansylcadaverine-positive cells as well as by the appearance of the autophagic markers Beclin and LC3II. Prolonging the treatment to 48 h, **2a** caused cytotoxicity through the activation of caspase-dependent apoptosis.

1. Introduction

Previously we have reported the synthesis of the complex polycyclic compounds **1a-h** containing the 5,7:7,13-dimethanopyrazolo[3,4-*b*]pyrazolo[3′,4′:2,3]azepino[4,5-*f*]azocine system (Fig. 1). The structure of these is characterized by a fused hexacyclic system that includes two *N*-phenyl-substituted pyrazole rings (A and B in Fig. 1) that stabilize the half-chair conformation of the adjacent two azepine rings (E and F in Fig. 1). Finally, these compounds have two fused five-membered rings (G and H in Fig. 1) [1–3].

Compounds **1a-g** were tested in vitro by the National Cancer Institute (NCI, Frederick, MD, USA) for their antiproliferative activity against a panel of 57 human cancer cell lines derived from nine clinically isolated cancer types (leukemia, lung, colon, melanoma, renal, ovarian, brain, breast and prostate). The most active compounds were **1d** and **1g**, bearing on each of the two phenyl rings a methoxy or glucose-containing moiety, respectively. Both of these moieties could be involved in hydrogen bonds with a cell molecular target and produce lower partition coefficient values than the inactive compounds **1b,c,e**, which all have very high log P values (Table 1).

Moreover, comparing **1d** and **1g**, the latter derivative was much more active than the former. In fact, it showed antiproliferative activity, expressed as a GI50 value (compound concentration that inhibits 50% net cell growth) in the range 0.29–5.43 μM against all the tumor cell lines of the NCI panel, and the mean graph midpoint (MG_MID, arithmetical mean value) calculated for LogGI50 (M) was −5.82 [3].

* Corresponding authors.
E-mail addresses: mariavaleria.raimondi@unipa.it (M.V. Raimondi), fabiana.plescia@unipa.it (F. Plescia).
[1] These authors contributed equally to this work.
[2] These authors contributed equally to this work.

https://doi.org/10.1016/j.bioorg.2020.103989
Received 18 February 2020; Received in revised form 25 April 2020; Accepted 29 May 2020
Available online 01 June 2020

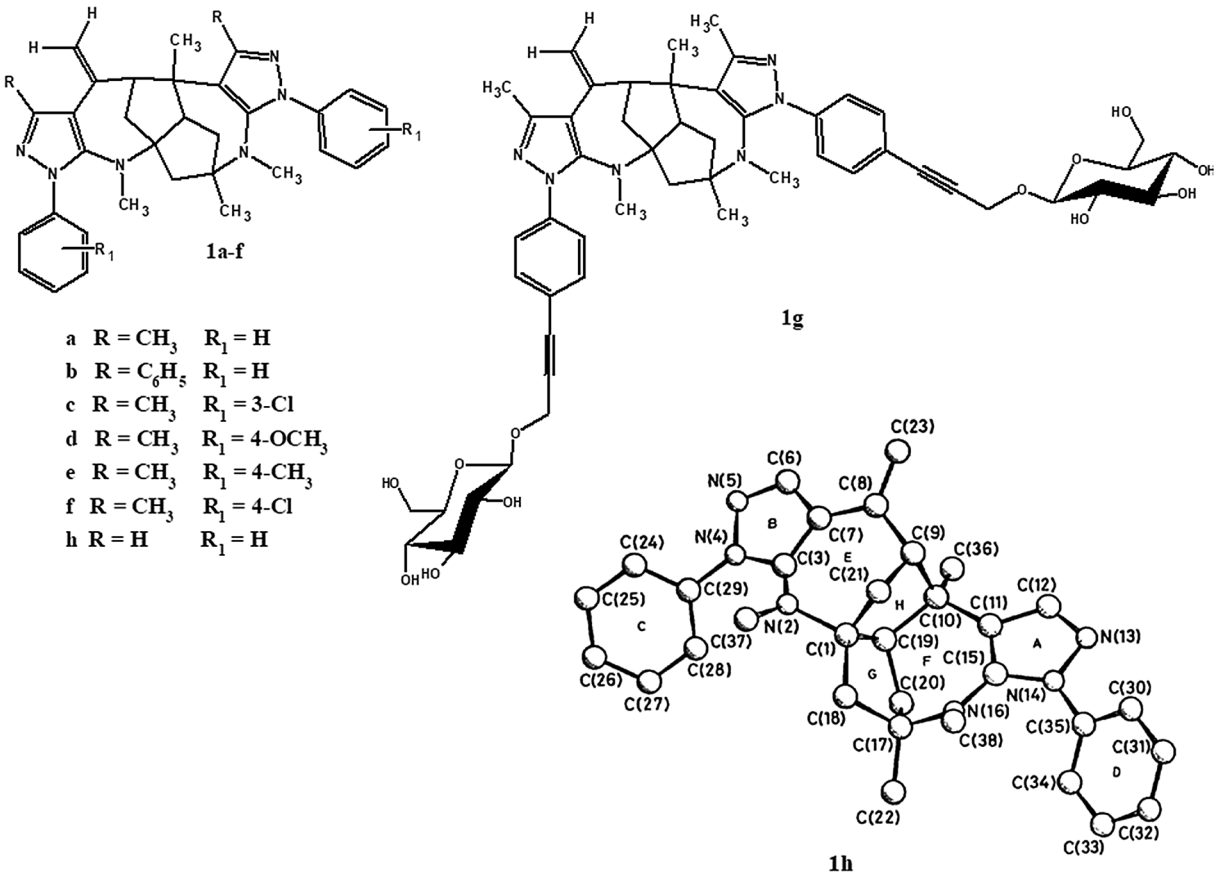

Fig. 1. Compounds **1a-h** and X-ray perspective of **1h.**

Table 1
Calculated log P values of previously synthesized compounds **1a-g.**

Compound	log P
1a	6.84 ± 1.32
1b	10.23 ± 1.68
1c	8.03 ± 1.33
1d	6.67 ± 1.48
1e	7.76 ± 1.32
1f	8.03 ± 1.33
1g	3.11 ± 1.51

For compound **1d,** the GI50 values were instead in the 1.18–11.3 μM range, and the mean graph midpoint value for LogGI50 (M) was −5.50 [2].

At this point, in order to obtain new polycyclic derivatives with greater hydrophilic character than **1d**, as well as to gain more insight into the role of the glucose-containing moiety of **1g**, we prepared new polycyclic derivatives **2a,b,c**, which bear on each of the phenyl rings the hydrophilic groups OH, SO_2NH_2, or $NHCOCH_3$ (Fig. 2).

Finally, we wanted to determine whether the two phenyl groups of polycycle **1a** could be replaced with methyl groups (compound **3**, Fig. 3) because this change decreased the partition coefficient value and therefore might enhance antiproliferative activity.

2. Results and discussion

2.1. Chemistry

The synthesis of polycyclic derivatives **2a-c** and **3** (Figs. 2 and 3) was performed as described in Schemes 1–3. The polycycle **2a** (Scheme 1) was obtained starting from the 3,*N*-dimethylpyrazole-5-amine derivative **4**, which was demethylated by reaction in 24% aqueous hydrobromic acid under microwave (MW) irradiation to give **5**.

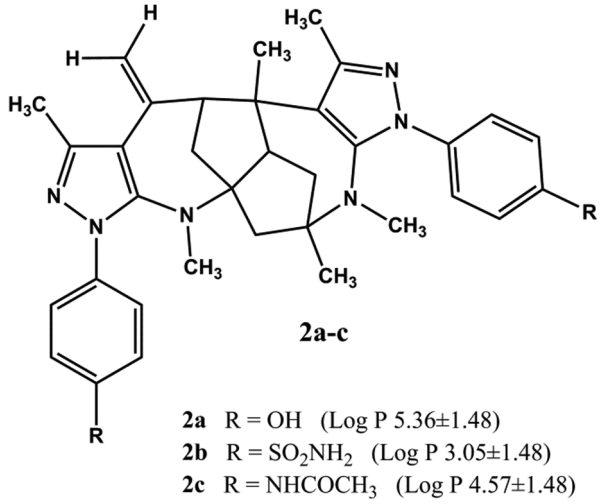

Fig. 2. Structures of compounds **2a-c.**

The latter compound was reacted with hexane-2,5-dione in 1,4-dioxane and in the presence of *p*-toluenesulfonic acid to afford **2a**. Compound **2b** was obtained as described in Scheme 2.

The pyrazole-5-amine derivative **8**, bearing the 4-sulfamoylphenyl moiety, is known. It was obtained from 4-hydrazinylbenzenesulfonamide **6** and 3-iminobutanenitrile **7** by modifying the reported procedure [4]. The 3-methyl-1-(4-sulfamoylphenyl)-1*H*-pyrazole-5-amine **8** was formylated with 95% formic acid to give

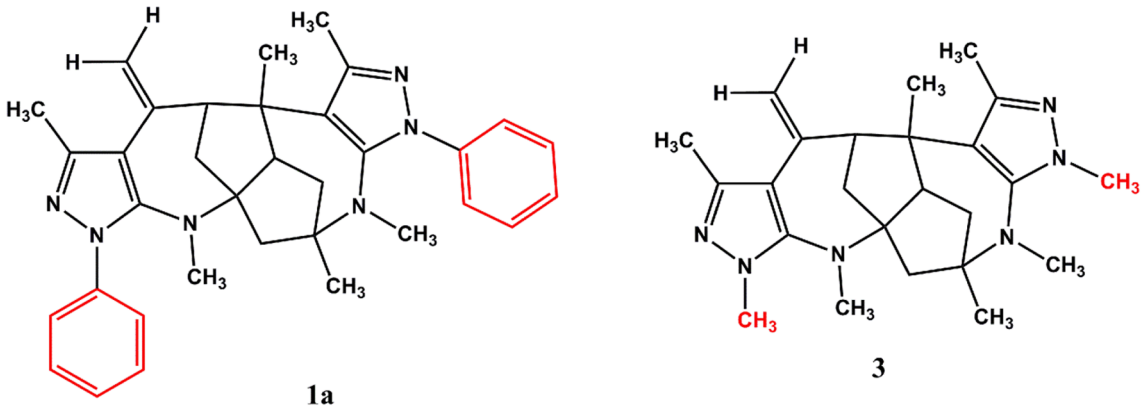

Fig. 3. Structure of compounds **1a** and **3**.

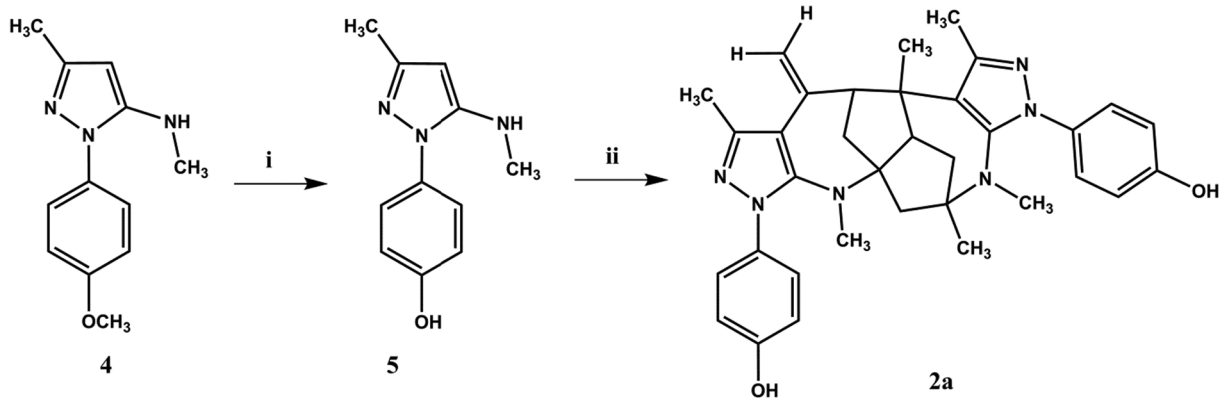

Scheme 1. Synthetic route to obtain compound **2a**: **i** HBr 24%, MW: 150 °C, 80 W, 6 cycles of 10 min each; **ii** hexane-2,5-dione, *p*-toluenesulfonic acid, reflux.

derivative **9**, which, in turn, was reduced with lithium aluminum hydride to afford the 3,*N*-dimethyl-1*H*-pyrazole-5-amine derivative **10**. Finally, the latter compound was reacted with hexane-2,5-dione in 1,4-dioxane, in the presence of *p*-toluenesulfonic acid, to give the polycyclic derivative **2b**.

Compound **2c** was prepared as described in Scheme 3, starting from the pyrazole derivative **11**, which was reduced by hydrogen and Pd/C to give the amino derivative **12**. The latter compound was treated with $LiAlH_4$ to afford compound **13**. The amino group linked to phenyl ring was protected by benzylchloroformiate to afford **14**, which was reacted with hexane-2,5-dione in 1,4-dioxane and in the presence of *p*-toluenesulfonic acid to yield the intermediate **15**. Compound **15** was deprotected to give **16**. Finally, **16** was acetylated by acetic anhydride to afford the desired polycycle **2c**.

Compound **3** was obtained as described in Scheme 5 by reacting 1,3,*N*-trimethyl-pyrazole-5-amine **17** with hexane-2,5-dione in dioxane and in the presence of *p*-toluenesulfonic acid to afford **3.**

Despite some differences in the experimental procedures to obtain the best yields of the synthesized products (Schemes 1–4), the reactions proceeded with the same mechanism of action. In particular, the formation of compounds **2a-c** and **3** can be hypothesized as described in scheme 5 for compound **2a**, taken as an example. The reaction between the *N*-methyl-1-phenyl-1*H*-pyrazol-5-amine **5** and the hexane-2,5-dione **18** in the presence of *p*-toluenesulfonic acid leads to the intermediate **19** containing a pyrazolo[3,4-*b*]azepine structure. The rearrangement of one molecule of **19**, by the action of a H^+ ion, gives a new enamine intermediate. This last reacts with another molecule of **19** to form a methylene bridge between the two structures. A further rearrangement of this adduct leads to the formation of **2a**.

The new compounds were identified on the basis of analytical as well as spectroscopic data. In particular, the structures of compounds **2a,b,c** and **3** were confirmed principally by NMR analysis. The ^{1}H NMR spectra of **2a,b,c** and **3** are highly complex and very similar to that of polycyclic compounds previously reported by us [1–3], and, as a consequence, we assigned to them the same skeleton structure. In Fig. 1 is shown the X-ray perspective of **1h** that can be taken as the stereochemical reference model for compounds **2** and **3**. The ^{13}C NMR (APT) spectra of compounds **2** and **3** confirmed the assigned structures.

2.2. Biological activity

The newly synthesized compounds **2a-c** and **3** were evaluated by the NCI against a panel of approximately 60 human cancer cell lines according to the NCI standard protocol [5], as had been compounds **1a-g** previously [2,3].

A mean value was calculated for percent of cell growth inhibition at a 10^{-5} M concentration, giving an average activity parameter for all the cell lines. The mean growth percent for the new derivatives **2a-c** and **3** are summarized in Table 2 along with the previously published [2,3] data obtained with **1a-g** for ease of comparison.

Our data (Table 1, Fig. 4) show that the best Mean Growth Percent values were obtained by compounds with log P values falling in the range 3.05–6.67. However, the greater hydrophilic character of **2a-c** as compared with **1d** produced a slight increase in antiproliferative activity only in the case of **2a**, whereas for **2b** and **2c** their anticancer activity was similar to that observed with **1d**.

Compound **3**, despite having the lowest log P value in this group of compounds, was among the least active. Apparently, replacing the two phenyl moieties with methyl groups led, perhaps, to the loss of some fundamental interactions with the biological target(s). The polycycle **2b** bears two sulfonamido groups as substituents, and it has a log P value of 3.05, similar to the value of 3.11 of **1g.** Despite these similar log P

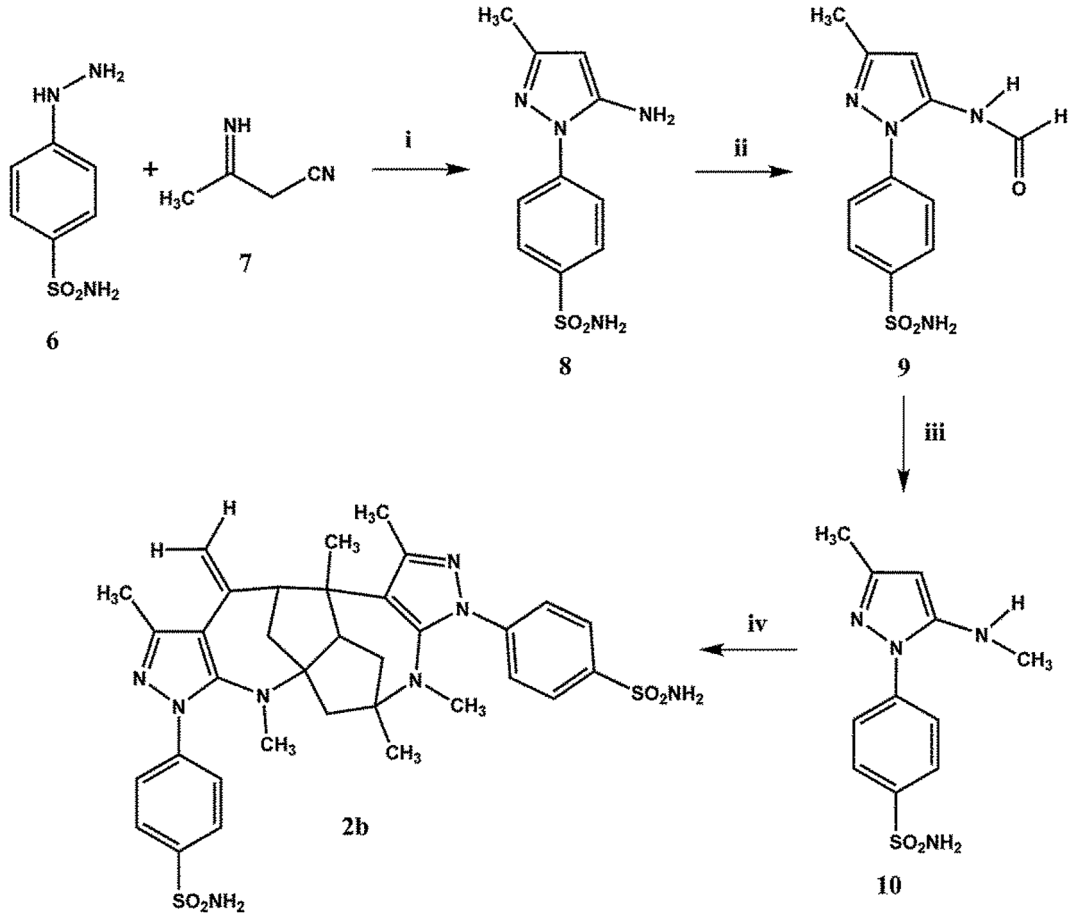

Scheme 2. Synthetic route to obtain compound **2b**: **i** 50 °C, 10 min; 37% aqueous HCl, 15 min, reflux, NaOH; **ii** 95% formic acid, reflux; **iii** $LiAlH_4$; **iv** hexane-2,5-dione, *p*-toluenesulfonic acid, reflux.

values, **1g** was significantly more active than **2b**.

These data thus support the hypothesis that the glucose moieties of **1g** might play a role in the transport of **1g** into the cancer cells. In support of this idea, it is well documented that the majority of cancer cells, to satisfy their high glucose requirement, increase their glucose uptake by overexpressing a family of facilitative glucose transporters (GLUTs) [6,7]. In this context, the glucose moieties of **1g** might be an effective substrate for these glucose transporters [3,8].

2.2.1. Compound *2a* reduced viability of MDA-MB231 breast cancer cells

To gain insight into the mechanism of action of **2a**, the compound with the greatest antiproliferative activity, we evaluated its effect on MDA-MB231 cells, a triple-negative breast cancer cell line. MDA-MB231 cells were treated with various doses of compound **2a** for different times, and cell viability was evaluated with the 3-(4,5-dimethylthiazol-2-yl)-2,5-diphenyl tetrazolium bromide (MTT) assay. We found that **2a** strongly reduced MDA-MB231 cell viability in a time- and dose-dependent manner (Fig. 5A). A modest reduction of viability was observed in the first 24 h of treatment when a decrease of only 24% and 35% of control was observed with 15 and 20 μM compound **2a**, respectively. Prolonging the treatment time resulted in a further significant reduction in the viability of the cells, so that at 48 h a reduction of viable cells by 55% and 80% of control occurred with 15 and 20 μM compound **2a**, respectively.

The observation of MDA-MB231 cells under light microscopy showed clear morphological changes in cells exposed to compound **2a**. In fact, as shown in Fig. 5B, control cells showed a clear epithelial-like morphology, phenotypically appearing as spindle shaped cells. In contrast, there was a marked reduction in cell number and in cell size after a 48 h treatment with 15 or 20 μM compound **2a**. To determine whether the reduction in cell number caused by compound **2a** on MDA-MB231 cells was related to cell death induction, we evaluated by flow cytometric analysis the effect of the compound on cell staining by propidium iodide (PI), a fluorescent dye that binds to DNA by intercalating between base pairs.

Since PI is a cell-impermeable dye that in isotonic conditions stains only nuclei of cells that have lost plasma membrane integrity, it is commonly used to detect dead cells. As shown in Fig. 5C, the percentage of PI-positive cells increased from 2.9% in control cells to 50.8% and 56.0% in MDA-MB231 cells treated with 15 or 20 μM compound **2a**, respectively, for 48 h, thus inducing significant cell death. Further, flow cytometric analyses were performed to investigate the distribution of cells in the different phases of the cell cycle. These studies showed that treatment of MDA-MB231 cells with compound **2a** did not induce significant changes in cell cycle distribution after a 24 h treatment, but a 48 h treatment did increase the proportion of cells in the sub-G0/G1 region, characteristic of apoptotic cells with fragmented DNA (Fig. 6).

2.2.2. Compound *2a* induced autophagy in MDA-MB231 cells

The analysis of the effects exerted by compound **2a** on MDA-MB231 cells showed that the compound had only a modest cytotoxic effect in the first 24 h of treatment. This raised the possibility that a survival mechanism was activated in a first phase of treatment.

Autophagy is a self-degradative process that is activated in response to many stresses, including nutrient deprivation, hypoxia and oxidative stress [9,10]. Through the elimination of intracellular aggregates and damaged organelles and the recycling of the breakdown products, autophagy plays important roles in cell survival [11,12]. The process is

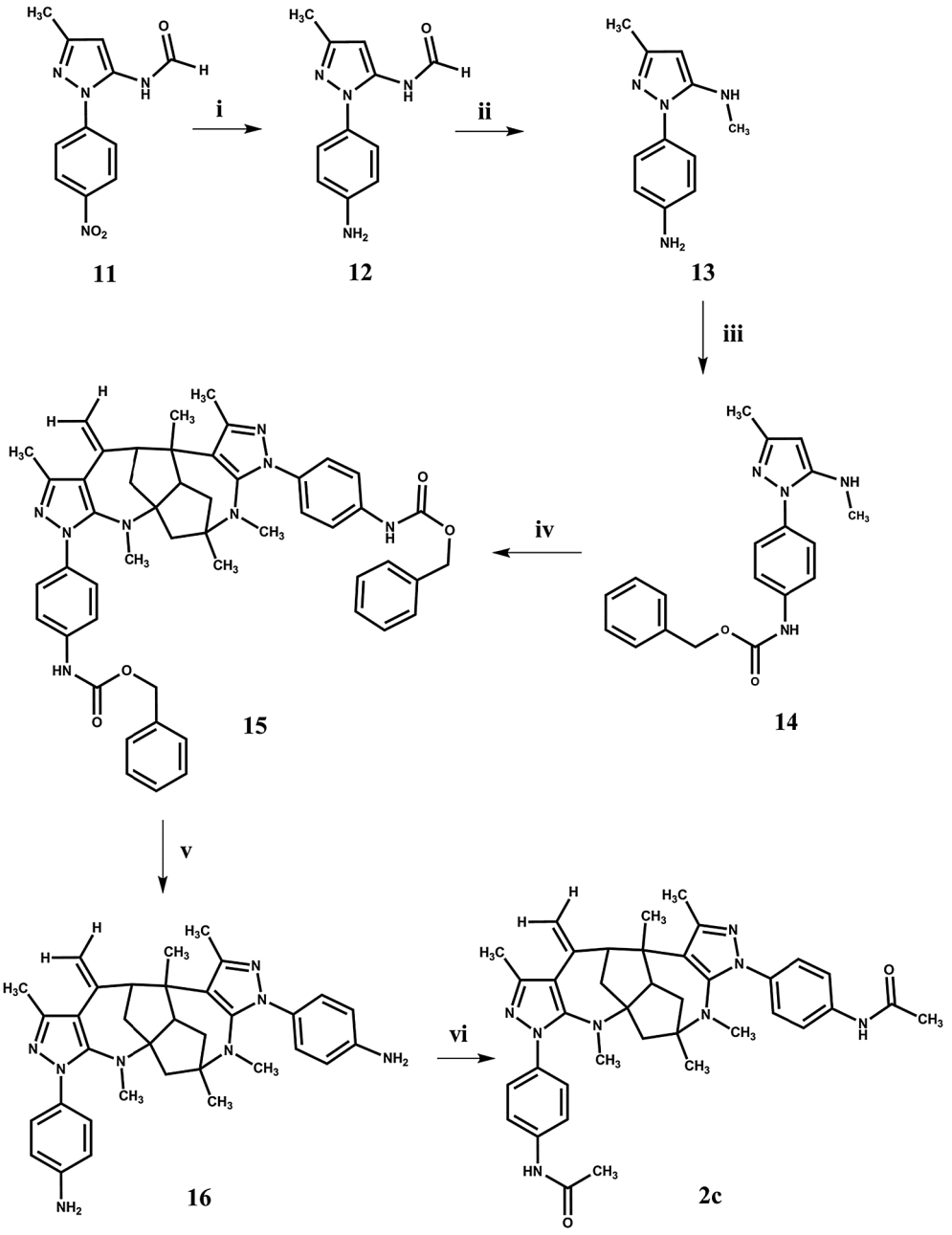

Scheme 3. Synthetic route to obtain compound **2c**: **i** H_2/Pd; **ii** $LiAlH_4$; **iii** NaOH 4 M, benzylchloroformiate; **iv** *p*-toluenesulfonic acid, hexane-2,5-dione, reflux; **v** EtOH/NaOH 6 M; **vi** acetic anhydride.

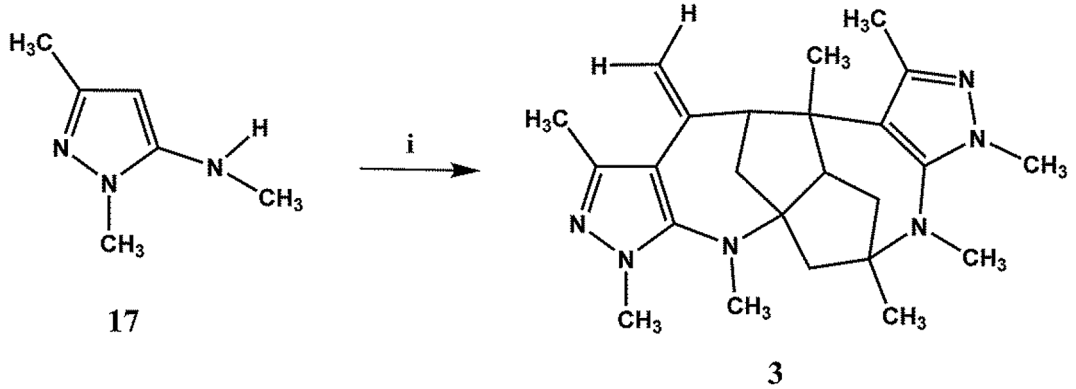

Scheme 4. Synthetic route to obtain compound **3**: **i** *p*-toluenesulfonic acid, hexane-2,5-dione, reflux.

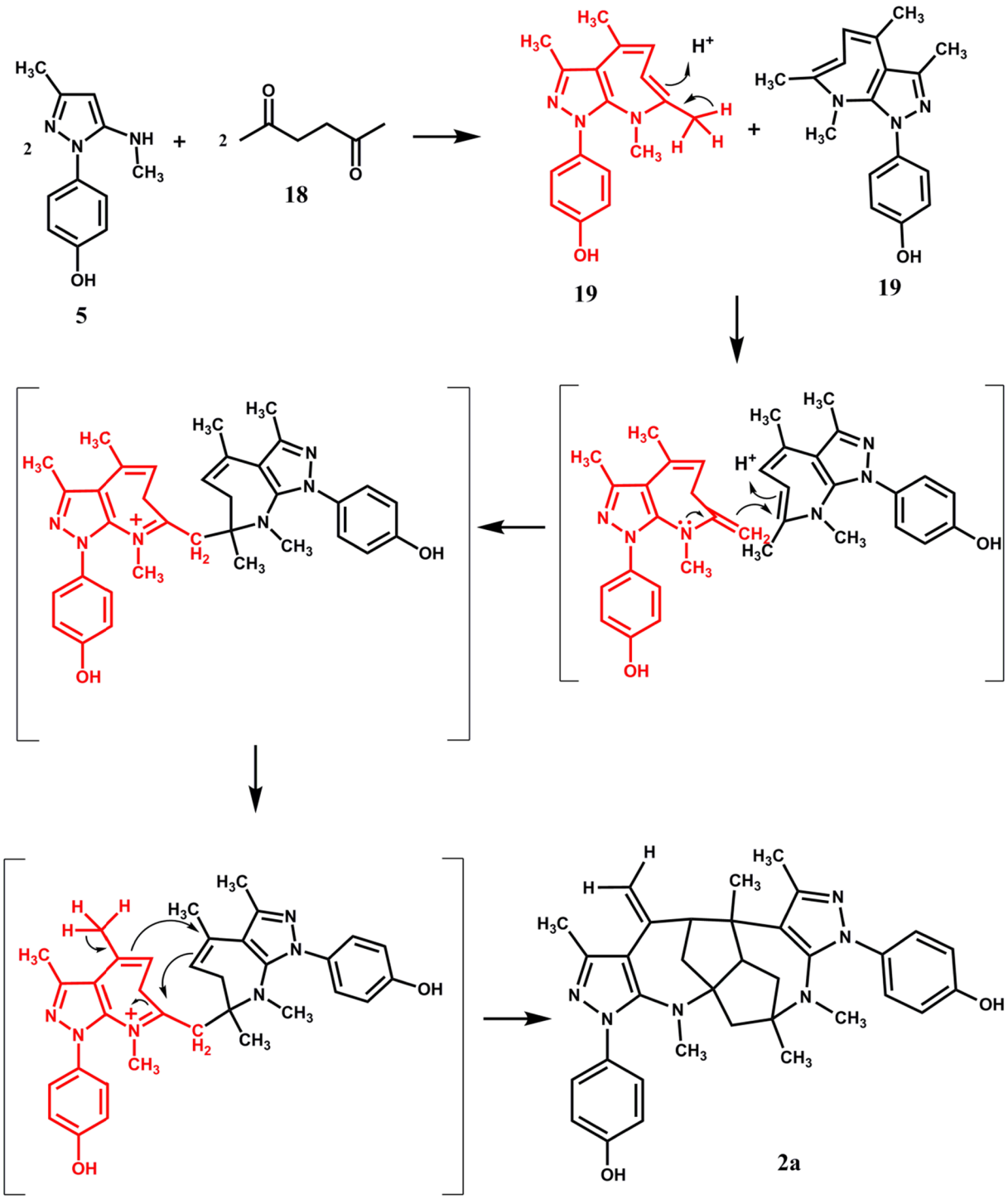

Scheme 5. Hypothesized mechanism of reaction leading to polycycle **2a.**

characterized by the formation of autophagic vacuoles (autophagosomes) that sequestrate portions of cytoplasm and fuse themselves with lysosomes, forming autolysosomes, to degrade the intra-autophagosomal components by lysosomal hydrolases [13].

The observation of cell morphology under light microscopy showed the appearance of vacuoles in MDA-MB231 cells treated for 24 h with compound **2a** (Fig. 7A, upper panels). To verify the presence of autophagic vacuoles, MDA-MB231 cells were stained with monodansylcadaverine (MDC), a fluorescent marker for autophagic vacuoles. Fig. 7A (lower panels) shows dot-like structures in the cytoplasm of compound **2a**-treated MDA-MB231 cells, suggesting the induction of autophagy. MDC-positive fluorescent cells were observed after a 24 h treatment with both 15 and 20 μM compound **2a**, with little analogous fluorescence in control cells.

Next, we analyzed the levels of the autophagic markers by Western blotting (Fig. 7B). Beclin is a protein that plays an essential role during the initiation of autophagy [14]. It is involved in autophagosome formation, and its expression increases during autophagy [14]. The data shown in Fig. 7B demonstrate that the Beclin protein level is significantly higher ($p < 0.001$) after a 24 h treatment with either 15 or 20 μM compound **2a** as compared to the untreated control.

Microtubule-associated protein light chain 3 (LC3) can be present in

Table 2
Overview of the results of the in vitro single high dose (10^{-5} M) antitumor screening for compounds **1-3**.[a]

Compound	log P	No. Studied[b]	% Mean Growth[c]
1a	6.84 ± 1.32	57	57.21
1b	10.23 ± 1.68	57	105.75
1c	8.03 ± 1.33	57	104.41
1d	6.67 ± 1.48	57	34.55
1e	7.76 ± 1.32	58	92.11[d]
1f	8.03 ± 1.33	nt	nt
1g	3.11 ± 1.51	56	0.74
2a	5.36 ± 1.48	55	29.90
2b	3.05 ± 1.48	55	36.87
2c	4.57 ± 1.48	55	36.34
3	2.94 ± 1.22	56	93.65

[a] Data obtained from the NCI's in vitro disease-oriented human tumor cell screen.
[b] Refers to the number of cell lines.
[c] Arithmetical mean value of growth percent (%MG) for all tested cancer cell lines.
[d] nt: not tested.

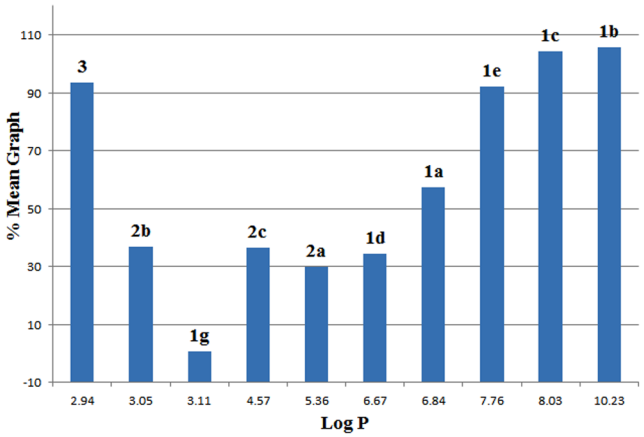

Fig. 4. Mean Growth Percent values versus log P for compounds **1a-e,g**, **2a-c** and **3.**

the cells in two different forms: LC3I, a soluble cytosolic form, and LC3II, a form conjugated with phosphatidylethanolamine and stably associated with autophagosome structure [15]. During the induction of autophagy, LC3I is cleaved to LC3II by the cysteine protease Atg4 and is recruited to autophagosomal membranes. As shown in Fig. 7B, Western blotting analysis demonstrated that treatment with compound **2a** favored the accumulation of LC3II ($p < 0.001$) with a concomitant reduction of LC3I.

2.2.3. Compound *2a* induced apoptosis in MDA-MB231 cells

The autophagic process is activated in response to cellular stress and, by improving the cell environment, it can represent a pro-survival mechanism. However, if the stress signal is very intense and persistent, the autophagic process cannot ensure cellular survival. If this is the case, the process can switch to apoptosis to eliminate damaged cells [12,16].

To investigate the activation of apoptosis in our experimental condition, cells were examined for the characteristic morphological features of apoptotic cell death by fluorescence microscopy. Using Hoechst 33342 to stain the nuclei, it was observed that, in comparison to normal cells, treatment with 15 or 20 μM compound **2a** induced, in a high percentage of MDA-MB231 cells, chromatin condensation and nuclear fragmentation, which are typical morphological changes occurring in apoptotic cell death (Fig. 8A). These results are in accordance with the increase in the proportion of cells in the subG0/G1 phase of the cell cycle that was observed in MDA-MB231 cells treated with compound **2a** for 48 h (Fig. 6).

Caspases are cysteine aspartyl proteases involved in the induction and execution of apoptotic cell death [17]. In healthy cells, these enzymes are present in inactive pro-caspase forms, which are activated into an active form by cleavage of a pro-domain.

The results shown in Fig. 8B demonstrate that, when MDA-MB231 cells were treated for 48 h with 15 or 20 μM compound **2a**, the intensity of the pro-caspase-9 band significantly ($p < 0.001$) decreased, suggesting the activation of the protease. Moreover, the decrease of pro-caspase-9 content was not observed after a 24 h treatment (Fig. 8B), thus confirming that the activation of apoptosis occurred only after a prolonged treatment time.

3. Conclusions

We synthesized novel polycyclic derivatives **2a-c** bearing on each of the two phenyl rings the hydrophilic groups OH, SO_2NH_2, or $NHCOCH_3$. These groups are more able than the OCH_3 group of **1d** to produce hydrogen bonds and to decrease the partition coefficient value of the compounds. The greater hydrophilic character of **2a-c** as compared with **1d** produced only a slight increase in antiproliferative activity and only in the case of **2a** (the activities of **2b** and **2c** were almost identical to that of **1d**). We also synthesized compound **3**, eliminating the two phenyl rings to produce an even more hydrophilic compound, but it was almost inactive at 10 μM. We conclude that replacing the phenyl moieties with methyl groups probably results in loss of interactions with the biological target.

Although derivative **2b** had a log P value (3.05) very similar to that of the glycoconjugate **1g**, the latter compound had a much higher antiproliferative effect than **2b** at 10 μM. This different activity supports the hypothesis that the glucose moiety of **1g** might be a substrate for GLUTs.

Finally, compound **2a**, the most active among the newly synthesized agents, was selected for further biological studies. Analysis of the effects of compound **2a** on triple negative MDA-MB231 breast cancer cells showed that **2a** activated within 24 h an autophagic response, demonstrated by the appearance of MDC-positive cells and the increase of the autophagic markers Beclin and LC3II. Prolonging the treatment to 48 h, compound **2a** induced an apoptotic cell death, as demonstrated by the activation of caspase-9.

4. Experimental

4.1. Chemistry

4.1.1. General

Reaction progress was monitored by TLC on silica gel plates (Merck 60, F254, 0.2 mm). Organic solutions were dried over Na_2SO_4. Evaporation refers to the removal of solvent on a rotary evaporator under reduced pressure. All melting points were determined on a Büchi 530 capillary melting point apparatus and are uncorrected. IR spectra were recorded with a Perkin Elmer Spectrum RXI FT-IR System spectrophotometer, with compound as a solid in a KBr disc or nujol. ^1H NMR (300 MHz) and APT (75 MHz) spectra were recorded with a Bruker AC-E spectrometer at r.t.; chemical shifts (δ) are expressed as ppm values. Microanalytic data (C, H, N) were obtained with an Elemental Vario EL III apparatus and were within ± 0.4% of the theoretical values. Yield refers to purified products and is not optimized. Log P values were calculated with the ACD/ChemSketch 14.01 2012 freeware version. The names of the compounds were obtained using ChemDraw Ultra 12.0 software (CambridgeSoft).

4.1.2. Procedure to prepare *4-[3-methyl-5-(methylamino)-1H-pyrazol-1-yl]phenol* ***5***

To a solution of 1-(4-methoxyphenyl)-*N*,3-dimethyl-1*H*-pyrazol-5-

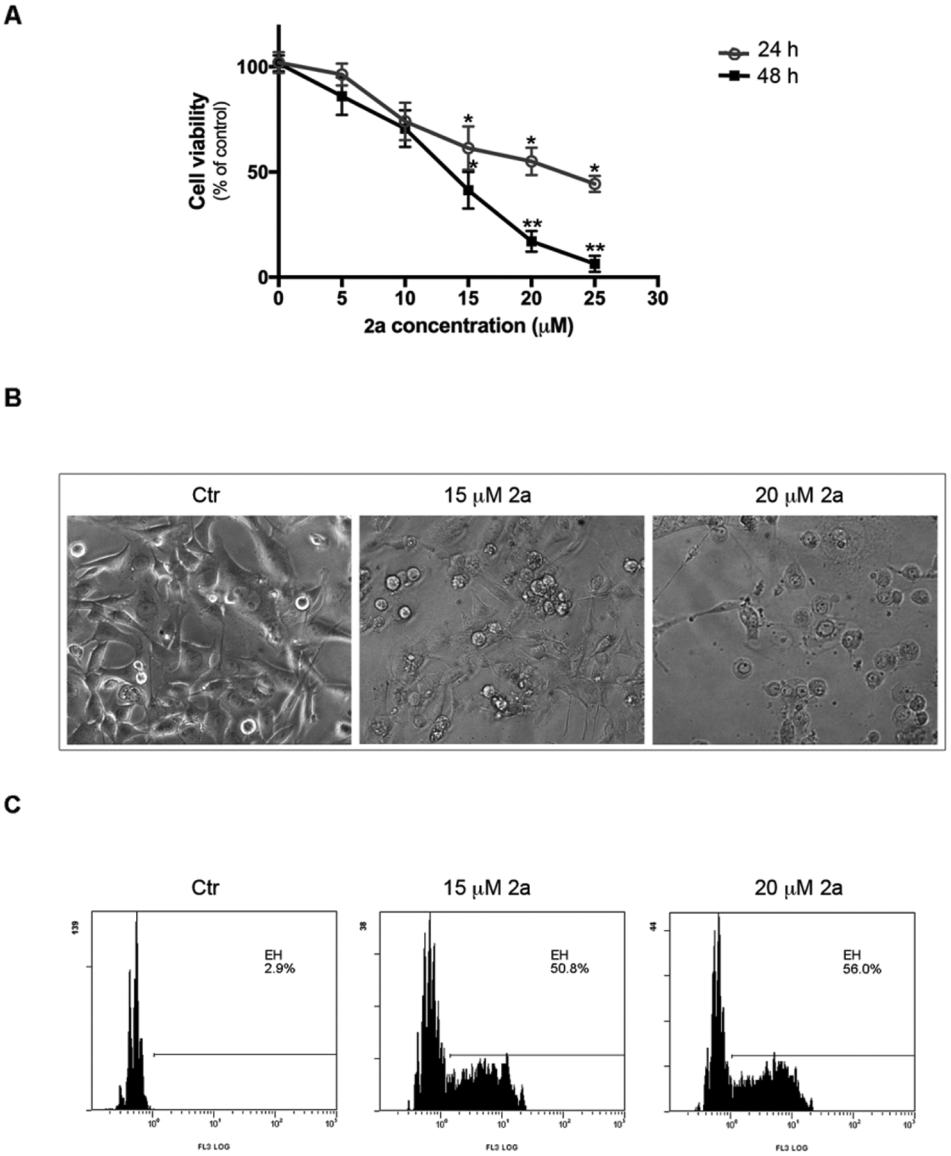

Fig. 5. *Effects of compound **2a** on viability of MDA-MB231 breast cancer cells.* (A) Cells (8×10^3) were treated with various doses of compound **2a** (5–25 μM) for 24 or 48 h. Cell viability was assessed by the MTT assay. Values are the means of three independent experiments ± S.D. (*) $p < 0.05$, (**) $p < 0.01$ compared to the control. (B) Effects of compound **2a** on the morphology of MDA-MB231 cells after treatment for 48 h with compound **2a**. (C) Flow cytometric analysis of dead cells using PI staining after a 48 h incubation with compound **2a**. Data are representative of three independent experiments ± S.D.

amine **4** (0.150 g, 0.69 mmol) in toluene (4 mL), a 24% HBr aqueous solution (4 mL) was added. The reaction mixture was irradiated with a MW power of 80 W at 150 °C for 10 min, and the MW cycle was repeated six times. The toluene was removed, and the solution was basified to pH = 8.5 with 40% aqueous NaOH. The white solid that precipitated was removed by filtration and crystallized from ethyl acetate to give **5** (0.073 g).

*4.1.2.1. 4-[3-methyl-5-(methylamino)-1H-pyrazol-1-yl]phenol (**5**).* 52% yield; mp 227–228 °C; IR (KBr) (cm^{-1}): 3482 (OH); 3350 (NH); ^1H NMR (DMSO-d_6) (δ) 2.09 (3H, s, CH_3); 2.63 (3H, s, NCH_3); 5.14 (1H, s, NH, exchangeable with D_2O); 5.28 (1H, s, pyrazole H-4); 6.84, 7.26 (4H, dd, C_6H_4); 9.59 (1H, s, OH, exchangeable with D_2O); ^{13}C NMR ($CDCl_3$) (δ) 14.32 (CH_3); 32.41 (NCH_3); 86.92 (pyrazole CH); 115.90 (2xCH); 125.51 (2xCH); 131.26 (C); 147.45 (C); 150.56 (C); 156.28 (C). Anal Calcd for $C_{11}H_{13}N_3O$: C, 65.01; H, 6.45; N, 20.68. Found: 65.15; H, 6.52; N, 20.62.

*4.1.3. Procedure to prepare 4,4′-{1,4,5,8,11,13a-hexamethyl-12-methylene-4,5,6,6a,8,12,13,13a-octahydro-5,7:7,13-dimethanopyrazolo [3,4-b]pyrazolo[3′,4′:2,3]azepino[4,5-f]azocine-3,9-diyl}diphenol **2a***

A solution of **5** (0.175 g, 0.86 mmol), 2,5-hexanedione (0.102 mL, 0.86 mmol) and *p*-toluenesulfonic acid monohydrate (20% mol/mol of **5**) in anhydrous dioxane was refluxed for 120 h. After the first 24 h, four portions of 2,5-hexanedione and *p*-toluenesulfonic acid monohydrate (50% of the above amounts) were added at intervals of 24 h.

Then, the solvent was removed under reduced pressure, and the oily residue was purified by flash chromatography [18] on silica gel (0.063–0.2 mm) (200 g): external diameter of the column 4.5 cm, ethyl acetate/cyclohexane (1:1) (1.3 L) as eluent. Fractions 21–25 (each 25 mL) were collected and evaporated to afford crude **2a** (0.01**1g**) as a white solid, which was crystallized from ethanol.

*4.1.3.1. 4,4′-{1,4,5,8,11,13a-hexamethyl-12-methylene-4,5,6,6a,8,12,13,13a-octahydro-5,7:7,13-dimethanopyrazolo[3,4-b] pyrazolo[3′,4′:2,3]azepino[4,5f]azocine-3,9-diyl}diphenol (**2a**).* 42% yield; mp 298 °C; IR (KBr) (cm^{-1}): 3450–3156 (broad band, OH); ^1H

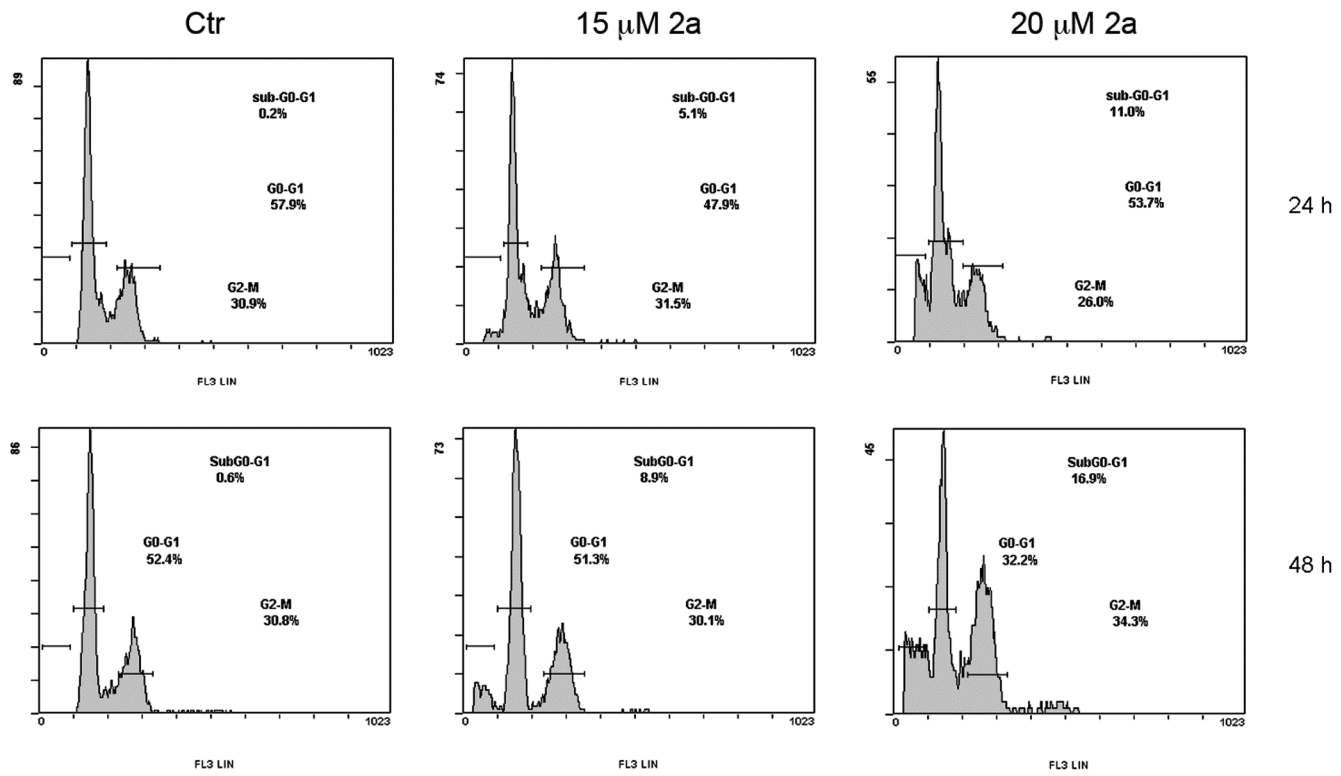

Fig. 6. *Effects of compound **2a** on cell cycle distribution of MDA-MB231 breast cancer cells*. Cells (1.5×10^4) were treated with 15 or 20 μM compound **2a** for the indicated times. Then, cells were centrifuged and resuspended in a hypotonic solution containing Nonidet-P-40 and PI. Cell cycle analysis by quantitation of DNA content was performed by flow cytometry using a Beckman Coulter Epics XL flow cytometer. At least 10,000 events were acquired for each condition. Histograms of the gated subG0/G1, G0/G1 and G2/M cells were analyzed by Expo32 software. Data are representative of three independent experiments.

NMR (DMSO-d_6) (δ) 1.16–2.67 (26H, a set of signals, 6xCH_3, 3xCH_2, 2xCH); 4.93, 4.98 (2H, br dd, methylene CH_2); 6.77–7.40 (8H, a set of signals, 2xC_6H_4); 9.59, 9.63 (2H, s, 2xOH, exchangeable with D_2O). ^{13}C NMR (DMSO-d_6) (δ) 15.17 (CH_3); 16.69 (CH_3); 23.85 (CH_3); 25.16 (CH_3); 34.41 (CH_3); 35.80 (CH_2); 36.02 (CH_3); 44.83 (CH_2); 46.49 (C); 55.91 (CH_2); 61.61 (CH); 66.33 (CH); 77.32 (C); 110.16 (C); 111.78 (CH_2, C); 115.25 (4xCH); 124.75 (2xCH); 124.99 (2xCH); 131.38 (C); 132.55 (C); 142.09 (C); 144.56 (C); 144.76 (C); 145.03 (C); 147.00 (C); 155.57 (C); 155.73 (C). Anal Calcd for $C_{34}H_{38}N_6O_2$: C, 72.57; H, 6.81; N, 14.94. Found: C 72.49; H, 6.85; N, 15.07.

*4.1.4. Procedure to prepare 4-(5-amino-3-methyl-1H-pyrazol-1-yl) benzenesulfonamide **8***

4-Hydrazinylbenzenesulfonamide **6** (5.000 g, 26.73 mmol) was solubilized in a mixture of H_2O (67.5 mL) and 37% HCl (2.8 mL), and the reaction was heated for 10 min at 50 °C. Then a solution of diacetonitrile **7** (1.800 g) in ethanol (22.5 mL) was slowly added. The reaction mixture was kept at 50 °C for another 10 min. After this time, 13.5 mL of 37% HCl was added, and the mixture was refluxed for 15 min, then cooled and basified to pH 8. A precipitate formed and was recovered by filtration (3.507 g). This was used for subsequent reactions without purification. Product **8** is known. Melting point, IR and ^1H NMR spectra were in agreement with those reported in the literature [6].

*4.1.5. Procedure to prepare N-[3-methyl-1-(4-sulfamoylphenyl)-1H-pyrazol-5-yl] formamide **9***

A mixture of **8** (2.830 g, 11.22 mmol) and 95% formic acid (12.7 mL) was refluxed with magnetic stirring for 2 h. After that time, the reaction mixture was neutralized with 40% aqueous NaOH. The precipitated solid was recovered by filtration, air-dried and crystallized from ethanol to give pure **9** (0.692 g).

*4.1.5.1. N-[3-methyl-1-(4-sulfamoylphenyl)-1H-pyrazol-5-yl]formamide (**9**).* 22% yield; mp 200–202 °C. IR (cm^{-1}): 3342 (NH), 3253 (NH_2), 1703 (CO); ^1H NMR δ: 2.22 (3H, s, CH_3); 6.38 (1H, s, pyrazole H-4); 7.56 (2H, br s, NH_2, exchangeable with D_2O); 7.71–7.92 (4H, dd, C_6H_4,); 8.20 (1H, s, CHO) 10.37 (1H, s, NH, exchangeable with D_2O). Anal Calcd for $C_{11}H_{12}N_4O_3S$: C, 47.14; H, 4.32; N, 19.99. Found: C 46.80; H, 3.95; N, 20.26.

*4.1.6. Procedure to prepare 4-[3-methyl-5-(methylamino)-1H-pyrazol-1-yl]benzenesulfonamide **10***

To a suspension of lithium aluminum hydride (0.420 g, 11.07 mmol) in anhydrous tetrahydrofuran (15 mL), a suspension of **9** (1.000 g, 3.50 mmol) in anhydrous tetrahydrofuran (20 mL) was added with stirring. The mixture was refluxed for 4 h, then the excess lithium aluminum hydride was destroyed with methanol and water. The solvent was then removed at reduced pressure, and the solid residue was extracted 5 times with ethyl acetate (5x40 mL). The organic extract was evaporated under reduced pressure to give a residue that was crystallized from ethanol to give **10** (0.420 g).

*4.1.6.1. 4-[3-methyl-5-(methylamino)-1H-pyrazol-1-yl] benzenesulfonamide (**10**).* 45% yield; mp 224–30 °C. IR (cm^{-1}) 3373 (NH), 3281 (NH_2); ^1H NMR δ 2.11 (3H, s, CH_3); 2.65 (3H, d, CH_3); 5.38 (1H, s, pyrazole H-4); 5.74 (1H, q, NH, exchangeable with D_2O); 7.41 (2H, s, NH_2, exchangeable with D_2O); 7.73–7.88 (4H, dd, C_6H_4). Anal Calcd for $C_{11}H_{14}N_4O_2S$: C, 49.61; H, 5.30; N, 21.04. Found: C 49.75; H, 5.40; N, 21.16.

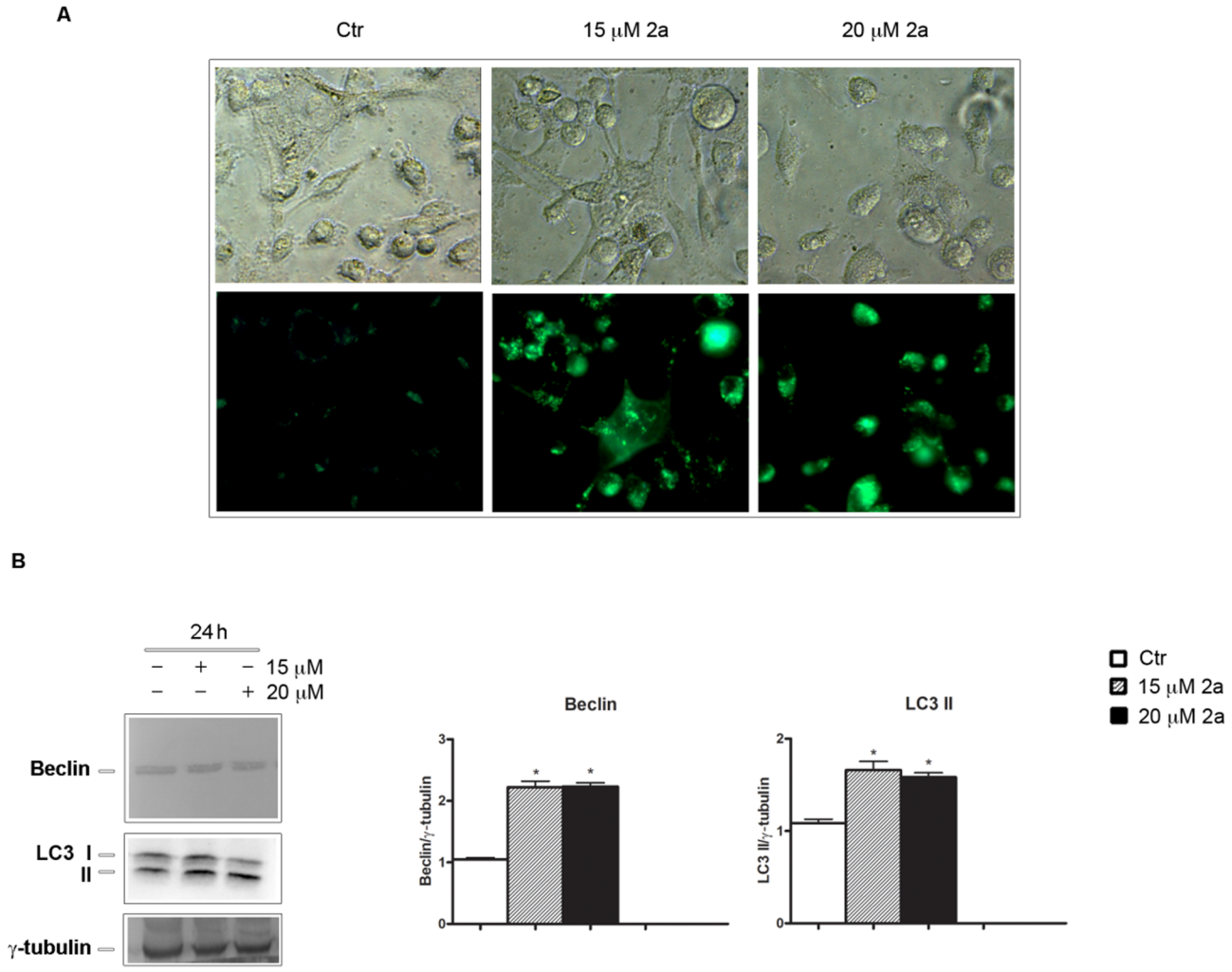

Fig. 7. *Compound **2a** treatment induced an autophagic flux in MDA-MB231 breast cancer cells.* (A) Cells (1.5×10^4) were treated with 15 or 20 μM compound **2a** for 24 h. The generation of the autophagic process was studied using MDC, a fluorescent dye that specifically labels the lysosomal/autophagic vacuoles. Fluorescence images were taken using a Leica DC300F microscope using a DAPI filter. At least three independent experiments were performed. A representative image (400 × original magnification) of the effects of **2a** treatment is shown. (B) Western blot analysis of autophagic markers Beclin and LC3 II in MDA-MB231 cells incubated in the presence or absence of compound **2a** (15 or 20 μM) for 24 h. All data were normalized to the housekeeping control represented by γ-tubulin. Densitometry analyses of each band, performed by ImageJ, were from three independent experiments and are shown in the center and right-hand panels (*) $p < 0.05$ compared to the untreated sample.

*4.1.7. Procedure to prepare 4,4′-{1,4,5,8,11,13a-hexamethyl-12-methylene-4,5,6,6a,8,12,13,13a-octahydro-5,7:7,13-dimethanopyrazolo [3,4-b]pyrazolo[3′,4′:2,3]azepino[4,5-f]azocine-3,9-diyl} dibenzenesulfonamide **2b***

To a suspension of **10** (0.590 g, 2.21 mmol) in anhydrous dioxane (12 mL), 2,5-hexanedione (0.26 mL, 2.21 mmol) and *p*-toluenesulfonic acid monohydrate (20% mol/mol of **10**) were added. The mixture was refluxed for 160 h. After the first 24 h of reflux, five portions of 2,5-hexanedione and *p*-toluenesulfonic acid monohydrate (50% of the above amounts) were added at intervals of 24 h. Then, the solvent was removed under reduced pressure and the residue treated with ethanol (4 mL). From the solution, left at room temperature for 24 h, a solid formed, and this was recovered by filtration and crystallized from DMF/H_2O (0.244 g).

4.1.7.1. 4,4′-{1,4,5,8,11,13a-hexamethyl-12-methylene-4,5,6,6a,8,12,13,13a-octahydro-5,7:7,13-dimethanopyrazolo[3,4-b] pyrazolo[3′,4′:2,3]azepino[4,5-f]azocine-3,9-diyl}dibenzenesulfonamide (2b). 16% yield; mp: 312 °C. IR (cm^{-1}): 3286 (NH_2); ^{1}H NMR (DMSO-d_6) (δ): 1.19–2.89 (multiple signals, 26H, CH_3, CH_2, CH); 5.06 (d, 2H, CH_2); 7.43 (s, 4H, exchangeable with D_2O, 2xNH_2); 7.71–7.95 (a set of signals, 8H, 2 × C_6H_4,). ^{13}C NMR (DMSO-d_6) (δ): 15.26 (CH_3); 16.75 (CH_3); 23.64 (CH_3); 24.96 (CH_3); 35.23 (CH_3); 36.58 (CH_3); 44.50 (CH_2); 46.55 (2xCH_2); 61.24 (CH); 61.61 (CH); 66.84 (2xC); 77.37 (2xC); 111.59 (CH_2); 112.89 (2xC); 122.16 (2xCH); 122.64 (2xCH); 126.67 (2xCH); 126.81 (2xCH); 140.90 (C); 141.28 (C); 142.09 (C); 143.03 (C); 145.39 (C); 146.99 (C); 147.27 (C); 147.55 (C). Anal Calcd for $C_{34}H_{40}N_8O_4S_2$: C, 59.28; H, 5.85; N, 16.27. Found: C 58.97; H, 5.54; N, 16.52.

*4.1.8. Procedure to prepare N-[1-(4-aminophenyl)-3-methyl-1H-pyrazol-5-yl]formamide **12***

To a solution of *N*-[3-methyl-1-(4-nitrophenyl)-1*H*-pyrazol-5-yl] formamide **11** (0.200 g, 0.81 mmol) in hot methanol (20 mL), 10% Pd/C (0.020 g) as a catalyst was added. The mixture was left under hydrogenation in a Parr apparatus at 50 psi for 20 h. After this time, the suspension was filtered, and the filtrate was evaporated to afford a solid that was crystallized to give **12** (0.128 g).

4.1.8.1. N-[1-(4-aminophenyl)-3-methyl-1H-pyrazol-5-yl]formamide (12). 64% yield; mp 201–202 °C (ethanol); IR (KBr) (cm^{-1}) 3391–3315 (multiple bands, NH_2 and NH), 1684 (CO); ^{1}H NMR

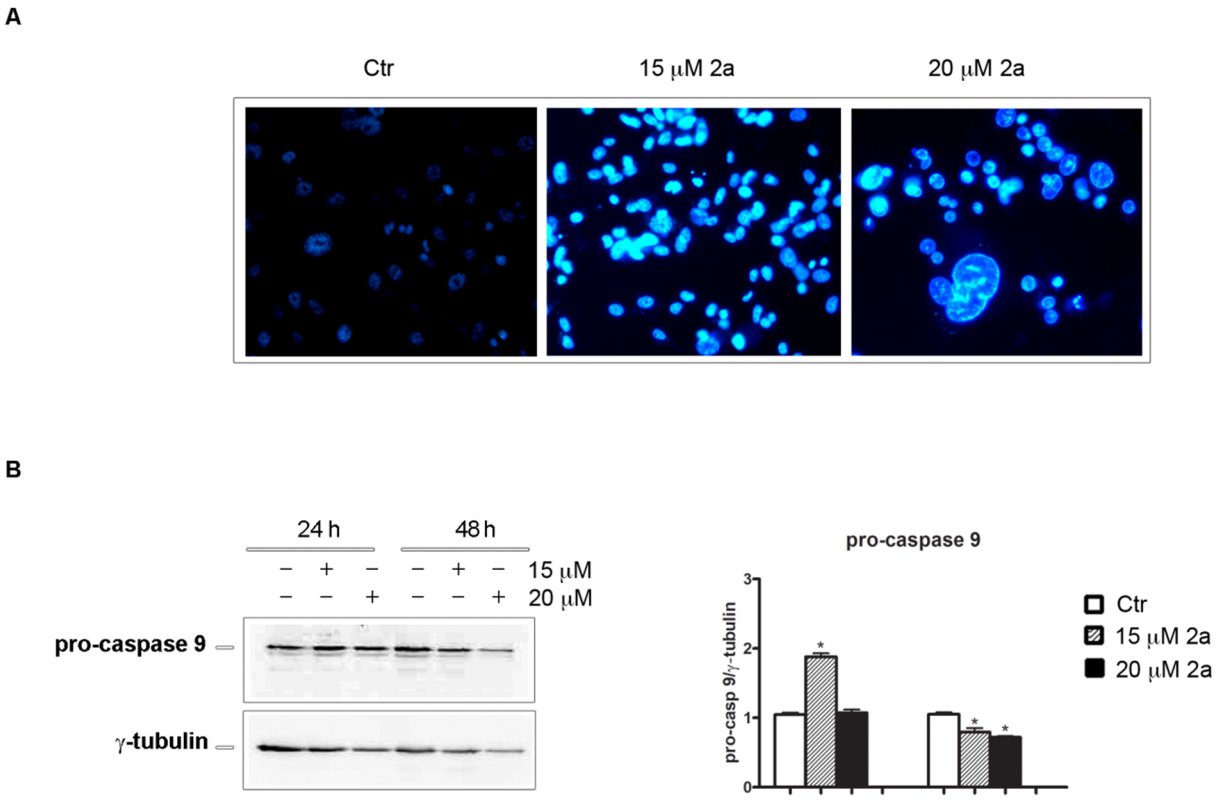

Fig. 8. *Prolonged treatment with compound **2a** induced DNA fragmentation and activation of caspase-9.* (A) Analysis of DNA condensation and fragmentation was evaluated by Hoechst 33342 staining after a 48 h treatment. Images (200x magnification) were acquired with a Leica fluorescent microscope using a DAPI filter. (B) Western blotting analysis of pro-caspase 9. Immunoblot was quantified by densitometry analysis and normalized against γ-tubulin. Results are from three independent experiments. (*) $p < 0.05$ compared to the untreated sample.

(DMSO-d_6) (δ) 2.16 (3H, s, CH_3); 3.58 (2H, br s, NH_2, exchangeable with D_2O); 6.32 (1H, s, pyrazole H-4); 6.62–7.06 (4H, dd, C_6H_4); 8.14 (1H, d, CHO), 10.02 (1H, br s, NH, exchangeable with D_2O). Anal Calc for $C_{11}H_{12}N_4O$: C, 61.10; H, 5.59; N, 25.91. Found: C 61.19; H, 5.65; N, 25.86.

*4.1.9. Procedure to prepare of 1-(4-aminophenyl)-N,3-dimethyl-1H-pyrazol-5-amine **13***

To a suspension of $LiAlH_4$ (0.110 g, 11 mmol) in anhydrous tetrahydrofuran (6.5 mL), compound **12** (0.200 g, 3.6 mmol) in anhydrous tetrahydrofuran (3.5 mL) was added slowly with vigorous stirring. The mixture was refluxed for 30 min. After this time, the excess $LiAlH_4$ was destroyed with ethanol and water, the organic solvent was evaporated under reduced pressure, and the aqueous phase was extracted with ethyl acetate (5 × 5 mL). Then, the solvent was removed under reduced pressure, and the oily residue was purified by flash chromatography [18] on silica gel (0.063–0.2 mm) (150 g): diameter of column bed 3.5 cm, ethyl acetate (1.3 L) as eluent. Fractions 29–39 (each 20 mL) were collected and evaporated, affording **13** (0.100 g) as a pure oil that solidified with ethanol.

*4.1.9.1. 1-(4-aminophenyl)-N,3-dimethyl-1H-pyrazol-5-amine (**13**).* 44% yield; mp 106–108 °C (ethanol); IR (KBr) (cm^{-1}) 3383–3235 (multiple bands, NH_2 and NH); ^{1}H NMR (DMSO-d_6) (δ) 2.05 (3H, s, CH_3); 2.59 (3H, d, NCH_3, J = 5.10 Hz); 4.98 (1H, apparent d, NH, exchangeable with D_2O); 5.20 (2H, br s, NH_2, exchangeable with D_2O); 5.21 (1H, s, pyrazole H-4); 6.57–7.06 (4H, a set of signals, C_6H_4). Anal Calcd for $C_{11}H_{14}N_4$: C, 65.32; H, 6.98; N, 27.70. Found: C 65.41; H, 7.05; N, 27.77.

*4.1.10. Procedure to prepare benzyl {4-[3-methyl-5-(methylamino)-1H-pyrazol-1-yl]phenyl}carbamate **14***

To a magnetically stirred cold solution (T = 0–5 °C) of **13** (0.270 g, 1.34 mmol) in a 2 M sodium hydroxide water/dioxane (1:1) (v/v) solution (2 mL), benzyl chloroformate (0.12 mL, 1.47 mmol) was added dropwise. Stirring was continued overnight at room temperature. Then the mixture was diluted with cold water and stirred until the formation of a solid. The product was removed by filtration and purified by flash chromatography on silica gel (0.063–0.2 mm) (150 g): diameter of column bed 3.5 cm, ethyl acetate/cyclohexane (1:1) (1.3 L) as eluent. Fractions 27–33 (each 20 mL) were collected and evaporated to afford **14** as a white solid, which was crystallized from ethyl acetate (0.340 g).

*4.1.10.1. Benzyl {4-[3-methyl-5-(methylamino)-1H-pyrazol-1-yl]phenyl} carbamate (**14**).* 75% yield; mp 72–74 °C; MS 337 (MH^+); IR (KBr) (cm^{-1}) 3383–3235 (multiple bands, 2xNH), 1684 (CO); ^{1}H NMR (DMSO-d_6) (δ) 2.08 (3H, s, CH_3); 2.61 (3H, d, NCH_3, J = 5.10 Hz); 5.16 (2H, s, CH_2); 5.28 (1H, s, pyrazole H-4); 5.32 (1H, apparent d, NH, exchangeable with D_2O); 7.38–7.55 (9H, a set of signals, C_6H_4 and C_6H_5); 9.90 (1H, br s, NH, exchangeable with D_2O). Anal Calcd for $C_{19}H_{20}N_4O_2$: C, 67.84; H, 5.99; N, 16.66. Found: C 67.91; H, 6.05; N, 16.67.

*4.1.11. Procedure to prepare benzyl {3-[9-(4-{[(benzyloxy)carbonyl] amino}phenyl)-1,4,5,8,11,13a-hexamethyl-12-methylene-5,6,6a,8,9,12,13,13a-octahydro-5,7:7,13-dimethanopyrazolo[3,4-b] pyrazolo[3′,4′:2,3]azepino[4,5-f]azocin-3(4H)-yl]phenyl}carbamate **15***

A solution of equimolar amounts of **14** (0.290 g, 0.86 mmol), 2,5-hexanedione (0.102 mL, 0. 86 mmol), and *p*-toluenesulfonic acid monohydrate (20% mol/mol of **14**) in anhydrous dioxane was refluxed for 120 h. After the first 24 h, four portions of 2,5-hexanedione and *p*-toluenesulfonic acid monohydrate (50% of the above amounts) were

added at intervals of 24 h. Then, the solvent was removed under reduced pressure, and the oily residue was purified by flash chromatography [18] on silica gel (0.063–0.2 mm) (200 g): diameter of column bed 4.5 cm, ethyl acetate/cyclohexane (1:1) (1.3 L) as eluent. Fractions 13–16 (each 25 mL) were collected and evaporated to afford a crude product that was crystallized from ethanol to give **15** as a white solid (0.150 g).

4.1.11.1. Benzyl {3-[9-(4-{[(benzyloxy)carbonyl]amino}phenyl)-1,4,5,8,11,13a-hexamethyl-12-methylene-5,6,6a,8,9,12,13,13a-octahydro-5,7:7,13-dimethanopyrazolo[3,4-b]pyrazolo[3′,4′:2,3]azepino[4,5-f]azocin-3(4H)-yl]phenyl}carbamate (15). 50% yield; mp 206–208 °C; IR (KBr) (cm^{-1}) 3324 (broad band, 2xNH), 1735 (2xCO); ^{1}H NMR ($CDCl_3$) (δ) 1.29–2.85 (26H, a set of signals, 6xCH_3, 3xCH_2, 2xCH); 5.01, 5.04 (2H, br dd, methylene CH_2); 5.22 (4H, s, 2× benzyl CH_2); 6.90 (2H, br s, 2xNH, exchangeable with D_2O); 7.34–7.63 (18H, a set of signals, 2xC_6H_4 and 2xC_6H_5). Anal Calcd for $C_{50}H_{52}N_8O_4$: C, 72.44; H, 6.32; N, 13.52. Found: C 72.49; H, 6.35; N, 13.57.

*4.1.12. Procedure to prepare 4,4′-{1,4,5,8,11,13a-hexamethyl-12-methylene-4,5,6,6a,8,12,13,13a-octahydro-5,7:7,13-dimethanopyrazolo[3,4-b]pyrazolo[3′,4′:2,3]azepino[4,5-f]azocine-3,9-diyl}dianiline **16***

To a solution of **15** (0.090 g, 0.11 mmol) in ethanol (3 mL), 6 M NaOH (0.9 mL) was added. After 30 min of reflux, the organic solvent was removed under reduced pressure to afford a solid product that was recovered by filtration. The solid was purified by flash chromatography [18] on silica gel (0.063–0.2 mm) (100 g): diameter of column bed 2.8 cm, ethyl acetate (1 L) as eluent. Fractions 30–54 (each 10 mL) were collected and evaporated affording a crude product as a white solid that was crystallized from ethanol to give pure **16** (0.038 g).

*4.1.12.1. 4,4′-{1,4,5,8,11,13a-hexamethyl-12-methylene-4,5,6,6a,8,12,13,13a-octahydro-5,7:7,13-dimethanopyrazolo[3,4-b]pyrazolo[3′,4′:2,3]azepino[4,5-f]azocine-3,9-diyl}dianiline **(16)***. 62% yield; mp 310–312 °C; IR (KBr) (cm^{-1}): 3437–3346 (multiple bands, 2xNH_2); ^{1}H NMR ($CDCl_3$) (δ) 1.15–2.68 (26H, a set of signals, 6xCH_3, 3xCH_2 and 2xCH); 3.43 (4H, br s, 2xNH_2, exchangeable with D_2O); 4.91, 4.96 (2H, br dd, methylene CH_2); 6.64–7.56 (8H, a set of signals, 2xC_6H_4); ^{13}C NMR ($CDCl_3$) (δ) 15.53 (CH_3); 16.74 (CH_3); 24.29 (CH_3); 25.65 (CH_3); 34.85 (CH_3); 36.45 (CH_3); 45.41 (CH_2); 47.05 (2xCH_2); 62.01 (CH); 62.20 (CH); 66.95 (2XC); 77.82 (2XC); 111.08 (C); 112.47 (CH_2); 115.02 (2xCH); 115.15 (2xCH); 125.12 (2xCH); 125.51 (2xCH); 129.89 (C); 130.56 (C); 142.45 (C); 145.01 (C); 145.55 (C); 145.75 (C); 145.93 (C); 146.26 (C); 147.66 (C). Anal Calcd for $C_{34}H_{40}N_8$: C, 72.83; H, 7.19; N, 19.98. Found: C 72.85; H, 7.18; N, 19.97.

*4.1.13. Procedure to prepare N,N′-{1,4,5,8,11,13a-hexamethyl-12-methylene-4,5,6,6a,8,12,13,13a-octahydro-5,7:7,13-dimethanopyrazolo[3,4-b]pyrazolo[3′,4′:2,3]azepino[4,5-f]azocine-3,9-diyl]bis(4,1-phenylene)}diacetamide **2c***

To a suspension of **16** (0.050 g, 0.09 mmol) in anhydrous dichloromethane (1.5 mL), acetic anhydride (0.019 mL) was added. After 30 min of reflux, the organic solvent was removed under reduced pressure, and the crude white solid that formed was recovered by filtration and washed with water. The solid was crystallized from ethanol to give **2c** (0.039 g).

*4.1.13.1. N,N′-{1,4,5,8,11,13a-hexamethyl-12-methylene-4,5,6,6a,8,12,13,13a-octahydro-5,7:7,13-dimethanopyrazolo[3,4-b]pyrazolo[3′,4′:2,3]azepino[4,5-f]azocine-3,9-diyl]bis(4,1-phenylene)}diacetamide **(2c)***. 68% yield; mp 300–301 °C; IR (KBr) (cm^{-1}) (CO); (multiple bands, 2xNH); ^{1}H NMR ($CDCl_3$) (δ) 1.28–2.81 (32H, a set of signals, 8xCH_3, 3xCH_2 and 2xCH); 5.01 (2H, br dd, methylene CH_2); 7.32–7.55 (8H, a set of signals, 2xC_6H_4); 8.69 (1H, s, NH, exchangeable with D_2O); 8.84 (1H, s, NH exchangeable with D_2O); ^{13}C NMR ($CDCl_3$) (δ) 15.38 (CH_3); 16.68 (CH_3); 20.93 (CH_3); 24.23 (2xCH_3); 25.83 (CH_3); 35.14 (CH_3); 36.63 (CH_3); 36.94 (CH_2); 39.32 (CH_2); 45.50 (CH_2); 47.20 (C); 62.07 (3xCH); 67.11 (C); 111.31 (C); 112.67 (C); 113.16 (CH_2); 120.07 (2xCH); 120.29 (2xCH); 124.10 (2xCH); 124.51 (2xCH); 135.50 (C); 135.87 (C); 136.86 (C); 137.14 (C); 141.89 (C); 146.20 (C); 146.86 (C); 147.13 (C); 147.83 (C); 169.24 (CO); 174.91 (CO). Anal Calcd for $C_{38}H_{44}N_8O_2$: C, 70.78; H, 6.88; N, 17.38. Found: C 70.85; H, 6.93; N, 17.45.

*4.1.14. Procedure to prepare 1,3,4,5,8,9,11,13a-octamethyl-12-methylene-3,4,5,6,6a,8,9,12,13,13a-decahydro-5,7:7,13-dimethanopyrazolo[3,4-b]pyrazolo[3′,4′:2,3]azepino[4,5-f]azocine **3***

To a solution of *N*,1,3-trimethyl-1*H*-pyrazol-5-amine **17** (0.950 g, 7.60 mmol) in anhydrous dioxane (19 mL), 2,5-hexanedione (0.89 mL, 7.60 mmol) and *p*-toluenesulfonic acid monohydrate (20% mol/mol of **17**) were added. The mixture was refluxed for 160 h. After the first 24 h, five portions of 2,5-hexanedione and *p*-toluenesulfonic acid monohydrate (50% of the above amounts) were added at intervals of 24 h. Then, the solvent was removed under reduced pressure, and the residue was chromatographed following the flash chromatography procedure [18] on silica gel (0.040–0.063 mm) (250 g): diameter of bed column 5.4 cm, ethyl acetate/cyclohexane (6:4 v/v) as eluent. Fractions 42–51 (each 50 mL) were collected and evaporated to afford a product that was crystallized from ethyl acetate to give **3** (0.556 g) as a colorless solid.

*4.1.14.1. 1,3,4,5,8,9,11,13a-octamethyl-12-methylene-3,4,5,6,6a,8,9,12,13,13a-decahydro-5,7:7,13-dimethanopyrazolo[3,4-b]pyrazolo[3′,4′:2,3]azepino[4,5-f]azocine **(3)***. 18% yield; mp: 212–214 °C; ^{1}H NMR ($CDCl_3$) (δ): 1.14 (s, 3H, CH_3); 1.37 (s, 3H, CH_3); 1.57–2.80 (multiple signals, 17H, 3xCH_3, 3xCH_2, 2xCH); 2.80 (s, 3H, CH_3); 3.65 (s, 6H, 2xCH_3); 4.92 (br signal, 2H, CH_2). ^{13}C NMR ($CDCl_3$) (δ): 15.22 (CH_3); 16.41 (CH_3); 24.02 (CH_3); 27.01 (CH_3); 34.98 (CH_3); 35.49 (CH_3); 35.96 (CH_2); 36.61 (CH_3); 37.30 (CH_3); 38.87 (CH_2); 45.15 (CH_2); 47.13 (C); 61.81 (CH); 62.08 (CH); 67.09 (C); 78.12 (C); 109.80 (C); 111.56 (CH_2); 112.42 (C); 142.43 (C); 144.56 (C); 145.22 (C); 147.24 (C); 148.05 (C). Anal Calcd for $C_{24}H_{34}N_6$: C, 70.90; H, 8.43; N, 20.67. Found: C 70.67; H, 8.64; N, 20.52.

4.2. Biology

4.2.1. Cell cultures

Triple negative breast cancer MDA-MB231 cells, obtained from Istituto Scientifico Tumori (Genoa, Italy), were grown as monolayers in culture medium (DMEM) supplemented with 10% (v/v) fetal bovine serum (FCS), 2 mM glutamine and 1% non-essential amino acids at 37 °C in a humidified atmosphere containing 5% CO_2 as previously described [19]. After plating on 96- or 6-well plates, cells were allowed to adhere overnight in culture medium before treatment with compounds. All reagents used for cell cultures were purchased from Euroclone (Pero, Italy).

4.2.2. Cell viability assay

To evaluate the effect of compound **2a** on cell viability, the MTT colorimetric assay was used as previously described [20]. MDA-MB231 cells (8×10^3/200 μL/well) were plated in 96-well plates and treated with various concentrations of **2a** for different times. Then, 20 μL MTT (11 mg/mL) was added, and the cells were incubated at 37 °C for 2 h. Finally, after removing the medium, 100 μL of lysis buffer (20% sodium dodecyl sulfate in 50% *N,N*-dimethylformamide) was added. At the end, the absorbance of the formazan was measured directly at 490 nm with 630 nm as a reference wavelength using an automatic ELISA plate reader (OPSYS MR, Dynex Technologies, Chantilly, VA). Cell viability was expressed as the percentage of the absorbance value of **2a**-treated cells compared with untreated samples used as control. Stock solutions of compound **2a** were prepared in dimethyl sulfoxide (DMSO) and diluted to final concentrations in DMEM. The concentrations of DMSO

used as vehicle never exceeded 0.04% and did not exert toxic effects on MDA-MD231 cells in comparison with the control. Each experiment was performed in triplicate.

Cell morphology images were acquired using an inverted Leica microscope equipped with a DC 300F camera (Leica Microsystems, Wetzlar, Germany).

In order to determine changes in nuclear morphology, MDA-MB231 cells were stained with Hoechst 33342, as previously described [21]. In particular, cells (7×10^3/well) were stained with Hoechst 33342 (2.5 μg/mL in medium) for 30 min, washed with phosphate-buffered saline (PBS), resuspended in culture medium and treated for various times with compound **2a**. A DAPI filter was used to examine cell morphology, and images were taken with a Leica DC 300F microscope (Leica Microsystems, Wetzlar, Germany) and acquired with Leica Q Fluoro Software.

Cell death was assessed by staining the cells with PI, a membrane impermeable dye generally excluded from viable cells. Cells were harvested, washed with PBS and incubated for 10 min at 4 °C in a solution of PBS containing 2 μg/mL PI. After staining, red fluorescence was measured using the FL3 channel using a 620-nm BP filter with a Coulter Epics XL flow cytometer (Beckman Coulter).

4.2.3. Flow cytometric analysis of cell cycle distribution

Cell cycle analysis was performed as previously described [21,22]. Cells were harvested by trypsinization and resuspended in a hypotonic solution containing 50 μg/mL PI, 0.1% sodium citrate, 0.01% Nonidet P-40 and 10 mg/mL RNase A. The cell cycle phase distribution was evaluated by an Epics XL flow cytometer (Beckman Coulter) using Expo32 software.

4.2.4. Western blot analysis

After treatment with **2a**, MDA-MB231 cells were lysed as described [23], and protein concentration was determined with the Bradford Protein Assay (Bio-Rad Laboratories S.r.L., Segrate, Milan, Italy). 40 μg of protein/sample were then separated by sodium dodecyl sulfate–polyacrylamide gel electrophoresis, after which the proteins were transferred to nitrocellulose membranes. Next, the nitrocellulose membranes were blocked with 1% milk-TBST (Tris-buffered saline, 0.1% Tween 20) and incubated overnight with 1 mg/mL of primary antibodies directed against Beclin (Santa Cruz Biotechnology, St. Cruz, CA), LC3 (Novus Biologicals, Littleton, CO), caspase-9 (Cell Signalling, Beverly, MA) or γ-tubulin (Sigma Aldrich, Milan, Italy). Membranes were then incubated with horseradish peroxidase-conjugated secondary antibody (1:5000) (Pierce, Thermo Fisher Scientific, UK), and the signals were detected using enhanced chemiluminescence (ECL) reagents (Cyanagen, Bologna, Italy). The signal obtained was visualized and photographed with Chemi Doc XRS (BioRad, Hercules, CA). The intensity of the bands was quantitated using Quantity One software (BioRad, Hercules, CA). Expression of proteins was normalized to γ-tubulin and compared to the appropriate controls. All the blots shown are representative of at least three separate experiments.

4.2.5. MDC test

To evaluate the formation of autophagic vacuoles, the MDC test was employed as described [16]. MDA-MB231 cells (8×10^3/200 μL culture medium) were plated in 96-wells plates and treated with **2a**. After the treatment, cells were incubated with 50 μM MDC for 10 min at 37 °C in the dark. Then, cells were washed with PBS and analyzed by fluorescence microscopy using a Leica DMR (Leica Microsystems) microscope equipped with a DAPI filter system (excitation wavelength of 372 nm and emission wavelength of 456 nm). Images were acquired by a computer-imaging system (Leica DC300F camera).

4.2.6. Statistical analysis

The statistical analysis of data was performed using the Student's *t* test and the one-way analysis of variance. All treated samples were compared to control (untreated) cells. The data are expressed as means ± SD. The statistical significance threshold was fixed at $p < 0.05$.

Declaration of Competing Interest

The authors declare that they have no known competing financial interests or personal relationships that could have appeared to influence the work reported in this paper.

Acknowledgements

This work was supported by Ministero dell'Istruzione dell'Università e della Ricerca (MIUR) of the Italian Government [grant numbers PJ_RIC_FFABR_2017_001683 and PJ_RIC_FFABR_2017_160599]. The authors wish to thank the Developmental Therapeutics Program of the National Cancer Institute of the United States of America for performing the antiproliferative screening of compounds in the 60 cell line assay. This research was supported in part by the Developmental Therapeutics Program in the Division of Cancer Treatment and Diagnosis of the National Cancer Institute, which includes federal funds under Contract No. HHSN261200800001E. The content of this publication does not necessarily reflect the views or policies of the Department of Health and Human Services, nor does mention of trade names, commercial products, or organizations imply endorsement by the U.S. Government.

Appendix A. Supplementary material

Supplementary data to this article can be found online at https://doi.org/10.1016/j.bioorg.2020.103989.

References

[1] G. Daidone, V. Sprio, S. Plescia, M.L. Marino, G. Bombieri, G. Bruno, Synthesis, molecular, and crystal structure of a new, unexpected polycyclic system: 5,12:10,12-dimethano-12*H*-pyrazolo[3,4-*b*]pyrazolo[4',3':6,7]azepino[2,3-*f*]azocine, J. Chem. Soc., Perkin Trans. 2 (1989) 137–141. The above polycyclic system name was erroneously reported in the above article title, the correct name is: 5,7:7,13-dimethanopyrazolo[3,4-*b*]pyrazolo[3′,4′:2,3]azepino[4,5-*f*]azocine.

[2] B. Maggio, D. Raffa, M.V. Raimondi, M.G. Cusimano, F. Plescia, S. Cascioferro, G. Cancemi, M. Lauricella, D. Carlisi, G. Daidone, Synthesis and antiproliferative activity of new derivatives containing the polycyclic system 5,7:7,13-dimethanopyrazolo[3,4-*b*]pyrazolo[3′,4′:2,3]azepino[4,5-*f*]azocine, Eur. J. Med. Chem. 72 (2014) 1–9.

[3] B. Maggio, M.V. Raimondi, D. Raffa, F. Plescia, M.C. Scherrmann, N. Prosa, M. Lauricella, A. D'Anneo, Synthesis and antiproliferative activity of a natural like glycoconjugate polycyclic compound, Eur. J. Med. Chem. 122 (2016) 247–256.

[4] B.E. Saatluo, M.M. Baradarani, J.A. Joule, Hexahydrospiro-pyrazolo[3,4-*b*]pyridine-4,10-pyrrolo[3,2,1-*ij*]quinolines derived from 5,6-dihydro-4*H*-pyrrolo[3,2,1-*ij*]quinoline-1,2-dione, J. Heterocyclic Chem. 55 (2018) 1176–1182.

[5] M.R. Boyd, K.D. Paull, Some practical considerations and applications of the National Cancer Institute *in vitro* anticancer drug discovery screen, Drug Dev. Res. 34 (1995) 91–109.

[6] M. Mueckler, B. Thorens, The SLC2 (GLUT) family of membrane transporters, Mol. Aspects Med. 34 (2013) 121–138.

[7] M.L. Macheda, S. Rogers, J.D. Best, Molecular and cellular regulation of glucose transporter (GLUT) proteins in cancer, J. Cell Physiol. 202 (2005) 654–1562.

[8] A. Diez-Sampedro, M.P. Lostao, E.M. Wright, B.A. Hirayama, Glycoside binding and traslocation in Na^+-dependent glucose cotransporters: comparison of SGLT1 and SGLT3, J. Membrane Biol. 176 (2000) 111–117.

[9] D. Carlisi, M. Lauricella, A. D'Anneo, G. Buttitta, S. Emanuele, R. di Fiore, R. Martinez, C. Rolfo, R. Vento, G. Tesoriere, The synergistic effect of SAHA and parthenolide in MDA-MB231 breast cancer cells, J. Cell Physiol. 230 (2015) 1276–1289.

[10] O. Pellerito, A. Notaro, S. Sabella, A. De Blasio, R. Vento, G. Calvaruso, M. Giuliano, WIN induces apoptotic cell death in human colon cancer cells through a block of autophagic flux dependent on PPARγ down-regulation, Apoptosis 19 (2014) 1029–1042.

[11] C. Cernigliaro, A. D'Anneo, D. Carlisi, M. Giuliano, A. Marino Gammazza, R. Barone, L. Longhitano, F. Cappello, S. Emanuele, A. Distefano, C. Campanella, G. Calvaruso, M. Lauricella, Ethanol-mediated stress promotes autophagic survival and aggressiveness of colon cancer cells via activation of Nrf2/HO-1 pathway, Cancers 11 (2019) 505.

[12] A. D'Anneo, D. Carlisi, M. Lauricella, R. Puleio, R. Martinez, S. Di Bella, P. Di Marco, S. Emanuele, R. Di Fiore, A. Guercio, R. Vento, G. Tesoriere, Parthenolide generates

reactive oxygen species and autophagy in MDA-MB231 cells. A soluble parthenolide analogue inhibits tumour growth and metastasis in a xenograft model of breast cancer, Cell Death Dis. 4 (2013) e891.
[13] F. Huang, B.R. Wang, Y.G. Wang, Role of autophagy in tumorigenesis, metastasis, targeted therapy and drug resistance of hepatocellular carcinoma, World J. Gastroenterol. 24 (2018) 4643–4651.
[14] M.B. Menon, S. Dhamija, Beclin 1 phosphorylation-at the center of autophagy regulation, Front. Cell Dev. Biol. 6 (2018) 137.
[15] J. New, S.M. Thomas, Autophagy-dependent secretion: mechanism, factors secreted, and disease implications, Autophagy 15 (2019) 1682–1693.
[16] S. Emanuele, A. Notaro, A. Palumbo Piccionello, A. Maggio, M. Lauricella, A. D'Anneo, C. Cernigliaro, G. Calvaruso, M. Giuliano, Sicilian litchi fruit extracts induce autophagy versus apoptosis switch in human colon cancer cells, Nutrients 10 (2018) 1490.
[17] S.H. MacKenzie, A.C. Clark, Death by caspase dimerization, Adv. Exp. Med. Biol. 747 (2012) 55–73.
[18] W.C. Still, M. Kahn, A. Mitra, Rapid chromatographic technique for preparative separations with moderate resolution, J. Org. Chem. 43 (1978) 2923–2925.
[19] M. Lauricella, A. Ciraolo, D. Carlisi, R. Vento, G. Tesoriere, SAHA/TRAIL combination induces detachment and anoikis of MDA-MB231 and MCF-7 breast cancer cells, Biochimie 94 (2012) 287–299.
[20] A. Marino Gammazza, C. Campanella, R. Barone, C. Caruso Bavisotto, M. Gorska, M. Wozniak, F. Carini, F. Cappello, A. D'Anneo, M. Lauricella, G. Zummo, E. Conway de Macario, A.J. Macario, V. Di Felice, Doxorubicin anti-tumor mechanisms include Hsp60 post-translational modifications leading to the Hsp60/p53 complex dissociation and instauration of replicative senescence, Cancer Lett. 385 (2017) 75–86.
[21] A. D'Anneo, D. Carlisi, M. Lauricella, S. Emanuele, R. Di Fiore, R. Vento, G. Tesoriere, Parthenolide induces caspase-independent and AIF-mediated cell death in human osteosarcoma and melanoma cells, J. Cell. Physiol. 228 (2013) 952–967.
[22] M. Lauricella, V. Lo Galbo, C. Cernigliaro, A. Maggio, A. Palumbo Piccionello, G. Calvaruso, D. Carlisi, S. Emanuele, M. Giuliano, A. D'Anneo, The anti-cancer effect of *Mangifera indica* L. peel extract is associated to γH2AX-mediated apoptosis in colon cancer cells, Antioxidants 8 (2019) 422.
[23] M. Lauricella, D. Carlisi, M. Giuliano, G. Calvaruso, C. Cernigliaro, R. Vento, A. D'Anneo, The analysis of estrogen receptor-α positive breast cancer stem-like cells unveils a high expression of the serpin proteinase inhibitor PI-9: Possible regulatory mechanisms, Int. J. Oncol. 49 (2016) 352–360.